Chalcogenide Letters Vol. 22, No. 12, December 2025, p. 1047-1053

Structural and Electrochemical Properties of Flower-Like SnS_2 Architectures as Cathodic Material for Lithium-Sulfur Batteries

N. Masood[1], A. M. Toufiq[2,*], S. Magam[3,4], S. M. W. Ali[2] and M. T. Qureshi[3,*]

[1]Chemistry Department, College of Science, University of Ha'il, Ha'il, 81451, Saudi Arabia
[2]Department of Physics, Hazara University Mansehra, Khyber Pakhtunkhwa, Mansehra, 21300, Pakistan
[3]Department of Basic Sciences, College of Preparatory Year, University of Ha'il, Ha'il, 55476, Saudi Arabia
[4]Department of Marine Chemistry and Pollution, Faculty of Marine Science and Environment, Hodeidah University, Hodeidah, P.O. Box 3114, Yemen
*Corresponding Authors: A. M. Toufiq. Email: arbabtoufiq@yahoo.com; M. T. Qureshi. Email: m.qureshi@uoh.edu.sa

Received: 11 September 2025; Accepted: 8 December 2025

ABSTRACT: Self-assembled highly hierarchical novel SnS_2 microflowers having acute edge nanopetals have been fabricated using a facile template-free hydrothermal growth technique utilizing Tin (II) chloride dihydrate ($SnCl_2 \cdot 2H_2O$) and Sodium sulfide nonahydrate ($Na_2S \cdot 9H_2O$) as reaction reagents. Morphological analysis exhibits the flower-type SnS_2 microarchitectures ranging from 4 to 7 μm. The vibrational mode measured at A_{1g} = 314 cm^{-1} confirms the existence of hexagonal phase SnS_2 using Raman spectroscopy. The electrochemical results suggest the promise of as-synthesized SnS_2 structures as a cathodic material in lithium-sulfur batteries.

KEYWORDS: Microflower nanoplates; hydrothermal synthesis; morphological studies; electrochemical data

1 Introduction

Recently, the nanoscale semiconductors have stimulated considerable attention [1,2]. The metal chalcogenide semiconductor nanomaterials have attracted extensive scientific and technological attention due to their unique optoelectronic properties [3,4], potential applications in solar cells [5], light-emitting diodes [6], photoconductors and semiconductors [7] and lithium-ion batteries [8]. The crystal structure of Tin (IV) disulfide consists of two-layered hexagonally closed packed anions of sulfur sandwiched with tin cations that are coordinated octahedrally by six nearest-neighbors of sulfur. An n-type semiconductor having a 2.44 eV band gap [9]. Various physio-chemical techniques have been utilized for synthesis of SnS_2 nanoparticles include solvothermal [10], chemical bath deposition [11], the hydrothermal process [12], thermo-decomposition [13], etc. Recently, metal sulfides have been also introduced into the cathode to enhance the electrochemical response of sulfur-based electrodes. SnS_2 is a highly conductive material among the transition metal sulfides and due to their capability as acting hosts. These guest species occupy the empty sites which are bounded by van der Waals forces between the adjacent closely packed layers of chalcogen [14]. Thus, lithium can be implanted into SnS_2 ascribing to the property and consequently, a cathode material, i.e., SnS_2 can be utilized for applications in lithium batteries [15]. Among alternative battery chemistries, rechargeable Li-S batteries using sulfur as cathode and Li as the anode gained attention due to their higher specific capacity, i.e., 1675 mAh/g and energy density (2600 Wh/kg) values. Their operating voltage is 2.1 V exhibits suitability for low-voltage electronic devices. Moreover, sulfur is low-cost, nontoxic and naturally abundant, making sulfur a potential candidate for Li-S batteries. Lithium ions are formed during discharge at the lithium-metal anode which transfer to the sulfur cathode through the electrolyte, similarly, the electrons move through an external circuit leading to the Li-S formation as the final cathodic discharge product [16]. SnS_2 is a highly conductive material produced at optimum temperatures where polysulfide clusters are created in sulfur-rich environment through sulfurization of Sn. A series of structural and compositional deviations occurs in Sulfur during cycling where

https://doi.org/10.15251/CL.2025.2212.1047

the insoluble sulfides and soluble polysulfides usually leading to losing active materials at the cathode, inferior coulombic efficiency and cycling stability in Li–S batteries. As a result, researchers are struggling to develop a stable electrode structure and adequate cycle life with improved efficiency. Despite of the significant progress, the efficiency and cycle-life still remain a challenge and limit their commercial use [17]. A stable reversible capacity higher than 600 mAh/g was obtained for tin sulfide electrodes [18]. Li et al. obtained SnS_2 stabilized sulfur in porous carbon composites and ensure a required cyclic stability of cathodes. A composite cathode of SnS_2 comprising sulfur (64.2%) can retain 924 mAh/g capacity in 200 cycles of charge/discharge at 0.2 C. Li et al. provided a design strategy of sulfur-hollow carbon nanosphere nanocomposite immobilized by tin sulfide which demonstrated excellent cyclic life and stability [19].

Here, a facile synthetic strategy and structural characterizations of SnS_2 microflowers using hydrothermal process is reported. This approach is easily scaled up and has great synthetic reproducible property. Moreover, the influence of reaction temperature on growth mechanism, rotational and vibrational modes using Raman spectroscopic technique and their lithium-sulfur battery features have been discussed.

2 Experimental Details

In this work, $SnCl_2{\cdot}2H_2O$, $Na_2S{\cdot}9H_2O$ along with thioglycolic acid (TGA) of analytical grade were used and these precursors. Typically, $SnCl_2{\cdot}2H_2O$ (0.0016 M) and Na_2S solution (160 mL) with a 0.08 M concentration were dissolved in ethylene glycol (20 mL) ultrasonically to form a homogeneous solution followed by addition of 80 μL of TGA to the solution under vigorous stirring for 20 min. The final mixture was shifted into 40 mL Teflon-lined autoclave and kept in the furnace for 24 h at 250°C. The final product was washed with distilled water and ethanol several times to remove the impurities before drying overnight at 80°C.

The phase identification and structural features were performed by X-ray diffractometer (Rigaku D/MAX-RB using Cu-Kα rad and λ = 1.54056 Å). Elemental analysis, structural and morphological characterizations were investigated using Energy-dispersive spectroscopy (INCA X-MAX 50, Abingdon, UK), Field-emission scanning electron microscopy FE-SEM (Zeiss Ultra 55, Jena, Germany) while the structural and vibrational features were examined using (Horiba Jobin Yvon HR 800, 532 nm) Raman spectroscopy. LAND electrochemical workstation was used for lithium-sulfur battery characteristics.

3 Results and Discussion

Fig. 1a shows the XRD spectra of SnS_2 architectures. Each diffraction peak observed in the spectra is well indexed to hexagonal SnS_2 berndtite with lattice parameters a = 0.3649 nm, c = 0.5899 nm and α = β = 90° and γ = 120° (JCPDF Card No. 23-0677). No other impurity peaks of SnS, Sn_2S_3 and Sn_3S_4 are observed. The presence of sharp and intense planes suggest that the prepared product is well crystallized. Furthermore, the calculated lattice parameters (a = 3.647 Å and c = 5.890 Å) of as-prepared SnS_2 are found in consistence with the standard values. The elemental composition of a single nanosheet measured through EDS analysis can be seen in the inset of Fig. 1b which confirms the XRD result and configuration of the pure SnS_2 structure.

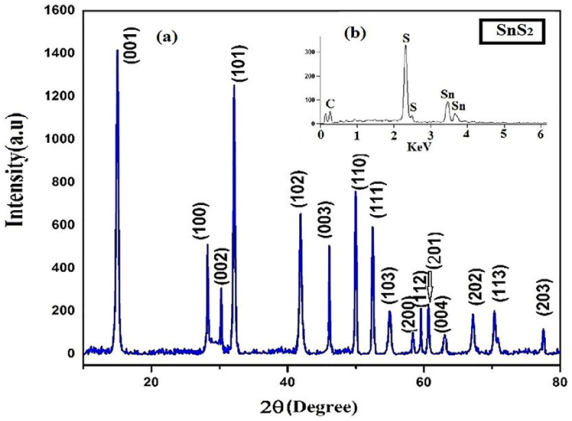

Figure 1: (**a**) X-ray diffraction spectra and (**b**) EDX of as-synthesized SnS_2 microstructure.

The morphology of tin disulfide was initially examined with the FESEM. The low magnification FESEM images as shown in Fig. 2a,b exhibits flower-like structure of the SnS_2 material and distributed over a carbon tape in the form of flower bouquets. Fig. 2c,d manifests high magnification image of single SnS_2 microflower and petals-like architectures, which reveals that the length of this flower is about 3–4 μm and sheet-like petals are 200–300 nm wide and several micrometers in length. A series of experiments were carried out at varying temperature to investigate the influence on growth of microflowers. The growth mechanism of SnS_2 flowers-like architectures in the range of 150–250°C is depicted in Fig. 3.

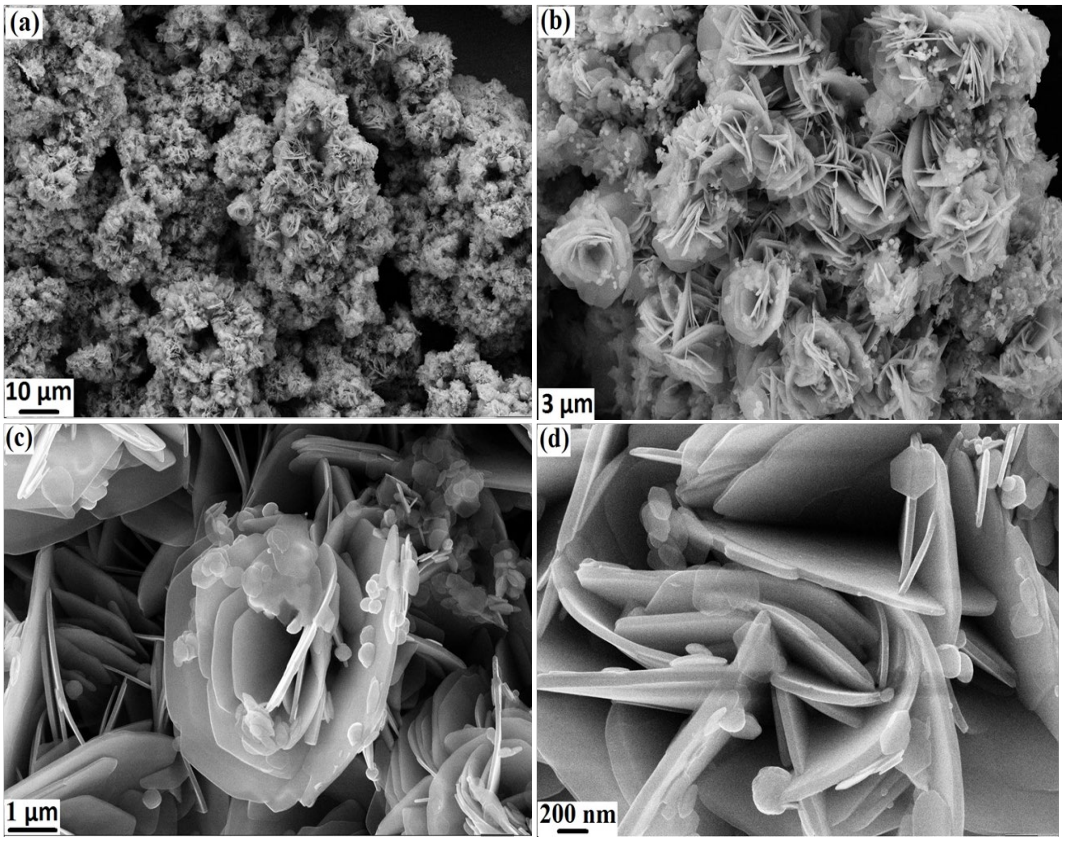

Figure 2: FESEM images (**a**,**b**) low magnification and (**c**,**d**) high magnification of SnS_2 microflowers.

These agglomerated nanoparticles (Fig. 3a) transform into flowers-like architecture after the addition of TGA. A hydrothermal route has been employed by Zhang et al. to fabricate metal sulfides using a template of thioglycolic acids (TGAs), revealing the role of TGA as aligned growth-reactant during the reaction [20]. The hydrothermal synthesis of flower-like nano/micro-crystal uses thioglycolic acid (TGA) as a stability agent to avoid agglomeration in chalcogenide nanocrystals.

The initial structure at low temperature (150°C) is displayed in Fig. 3a. The noticeable structural change as splitting view of microflowers can be seen by increasing the temperature to 200°C as shown in Fig. 3b. Finally, the structural disintegration becomes higher as to the complete arrangement of SnS_2 in to microflowers and by further increasing the temperature to 250°C, the surface of flowers gradually becomes smooth as shown in Fig. 3c.

Moreover, the structural and vibrational features of as-synthesized SnS_2 nanostructures were studied using Raman spectroscopy, which is a highly-advanced technique to study the chemical states and compositions. Fig. 4a shows the Raman spectra of SnS_2 flowers-like micro-architectures with a central peak observed at 314 cm^{-1} ascribing to A1g vibrations in SnS_2 and in good agreement with the reported literature [21,22].

Typical discharge-charge profiles of SnS_2 microflowers as cathodes are shown in Fig. 4b. For charge-discharge curves and cyclic performance, the current density of 0.5 C and potential window in the range 1.5–3 V were used. The first charge capacity is about 910 mAh/g and it can be seen that the microflowers exhibit an enhanced initial discharge capacity 900 mAh/g which is almost similar to the charge. Same phenomena of charge and discharge are observed for the charge-discharge profile which indicates the good and long-term stability of SnS_2 microflowers. The battery cyclic performance is shown in Fig. 4c. It is clear that after 150 cycles, discharge capacity still remains 590 mAh/g with 60% coulombic efficiency, which is higher than many reported values [23]. Zhou et al. reported that sulfur cathodes comprising SnS_2 with 191 $mAhg^{-1}$ and retention capacity of 31.3% demonstrate poor cycling stability at 0.5 C, with unstable coulombic efficiency and quick capacity degradation [24]. The improved cyclic performance and high coulombic efficiency can be attributed to the effective interaction between positively polarized Sn and negatively charged Polysulfides [15]. The better cyclic performance, the charge-discharge plateaus, and enhancement in the efficiency make SnS_2 microstructure a capable cathode material for Li-S batteries.

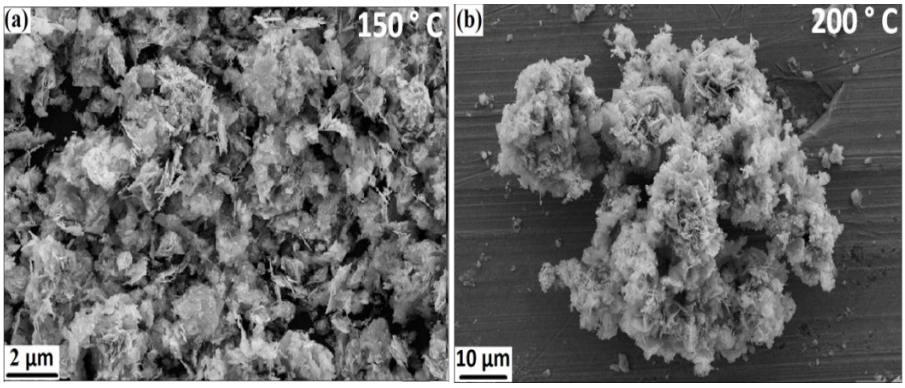

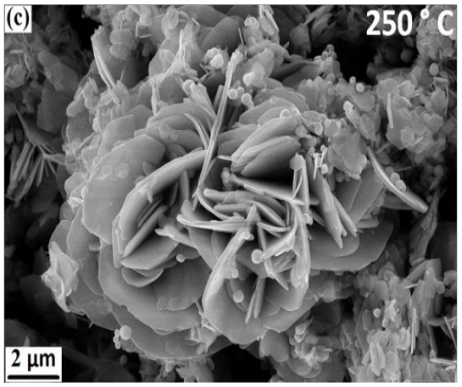

Figure 3: (**a**–**c**) growth mechanism of SnS_2 flowers-like microstructure at temperatures of 150°C, 200°C, and 250°C.

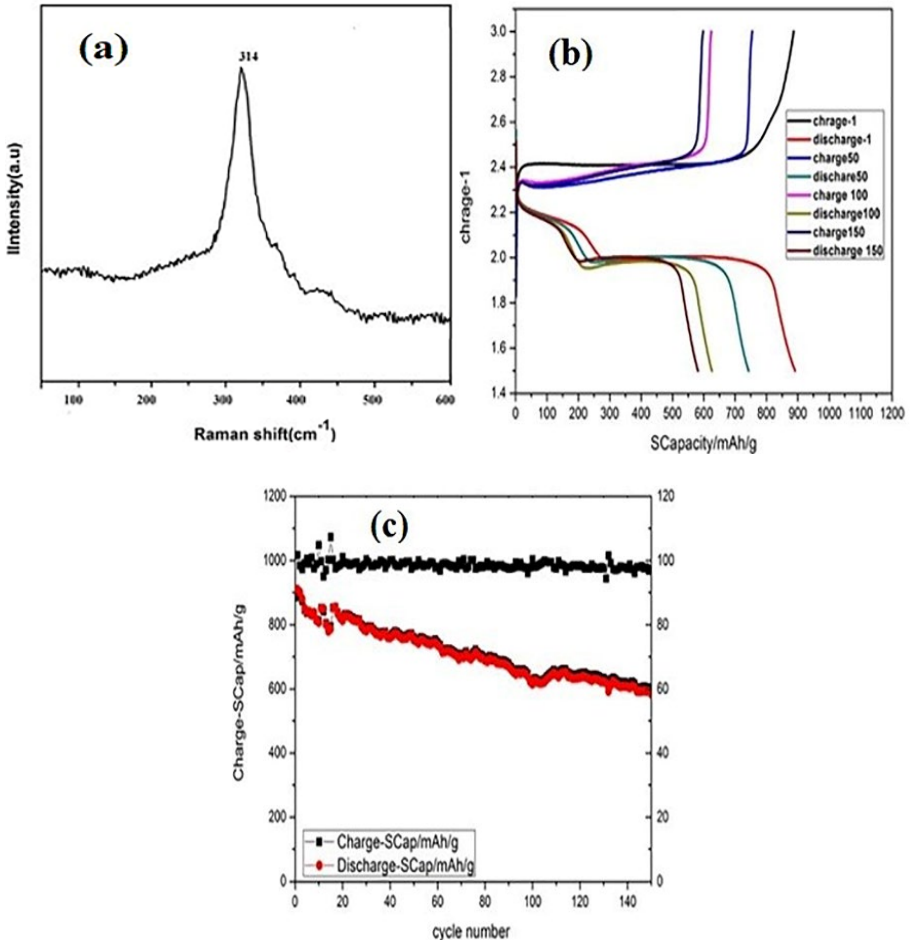

Figure 4: (**a**) Raman spectrum measured at 373 K (**b**) charge-discharge profile and (**c**) cyclic performance.

4 Conclusion

In conclusion, SnS_2 microflowers have been successfully fabricated using a hydrothermal growth template-free method. FESEM analysis reveal the flower-type architectures ranging from 4 µm to 7 µm, with an average nanopetal size in several hundred nanometer range. The evolution of flower-like morphologies reveals the formation of nanopetal arrangements with acute edges growing from the center towards the edges. Raman mode corresponding to A1g observed at 314 cm^{-1} confirms the

existence of hexagonal phase of SnS_2. The discharge-specific capacity was calculated to be about 900 mAh/g; during the first delithiation process was found to be 910 mAh/g, which is in accordance with the theoretical estimated values reported. The results suggest that our prepared material is potentially suitable for rechargeable Li-S batteries, the most capable high-energy density batteries (>600 $Whkg^{-1}$) and holds a great promise for large-scale grid energy storage applications and transportation.

References

1. Bawendi MG, Steigerwald ML, Brus LE. The quantum mechanics of larger semiconductor clusters ("quantum dots"). Annu Rev Phys Chem. 1990;41:477–96. https://doi.org/10.1146/annurev.pc.41.100190.002401.
2. Suryanarayanan R. Valence related optical and other studies of Sm and Tm chalcogenides. Phys Status Solidi (b). 1978;85:9–43. https://doi.org/10.1002/pssb.2220850102.
3. Tan F, Qu S, Zeng X, Zhang C, Shi M, Wang Z, et al. Photovoltaic effect of tin disulfide with nanocrystalline/amorphous blended phases. Solid State Commun. 2010;150:58–61. https://doi.org/10.1016/j.ssc.2009.10.006.
4. Zhang YC, Du ZN, Li SY, Zhang M. Novel synthesis and high visible light photocatalytic activity of SnS_2 nanoflakes from $SnCl_2{\cdot}2H_2O$ and S powders. Appl Catal B Environ. 2010;95:153–9. https://doi.org/10.1016/j.apcatb.2009.12.022.
5. Liu J, Li Y, Fan H, Zhu Z, Jiang J, Ding R, et al. Iron oxide-based nanotube arrays derived from sacrificial template-accelerated hydrolysis: large-area design and reversible lithium storage. Chem Mater. 2009;22:212–7. https://doi.org/10.1021/cm903099w.
6. Wang X, Li W, Sun K. Stable efficient CdSe/CdS/ZnS core/multi-shell nanophosphors fabricated through a phosphine-free route for white light-emitting-diodes with high color rendering properties. J Mater Chem. 2011;21:8558–65. https://doi.org/10.1039/c1jm00061f.
7. Raisin C, Bertrand Y, Robin J. Comparison of optical properties and band structures of $SnSe_2$ and SnS_2. Solid State Commun. 1977;24:353–6. https://doi.org/10.1016/0038-1098(77)90227-7.
8. Kim T-J, Kim C, Son D, Choi M, Park B. Novel SnS_2-nanosheet anodes for lithium-ion batteries. J Power Sources. 2007;167:529–35. https://doi.org/10.1016/j.jpowsour.2007.02.040.
9. Powell MJ. The effect of pressure on the optical properties of 2H and 4H SnS_2. J Phys C Solid State Phys. 1977;10:2967. https://doi.org/10.1088/0022-3719/10/15/029.
10. Vaughn DD, Hentz OD, Chen S, Wang D, Schaak RE. Formation of SnS nanoflowers for lithium-ion batteries. Chem Commun. 2012;48:5608–10. https://doi.org/10.1039/c2cc32033a.
11. Devika M, Reddy NK, Patolsky F, Ramesh K, Gunasekhar KR. Temperature dependent structural properties of nanocrystalline SnS structures. Appl Phys Lett. 2009;95:261907. https://doi.org/10.1063/1.3277148.
12. Xu Y, Al-Salim N, Bumby CW, Tilley RD. Synthesis of SnS quantum dots. J Am Chem Soc. 2009;131:15990–1. https://doi.org/10.1021/ja906804f.
13. Hickey SG, Waurisch C, Rellinghaus B, Eychmüller A. Size and shape control of colloidally synthesized IV–VI Nanoparticulate Tin(II) sulfide. J Am Chem Soc. 2008;130:14978–80. https://doi.org/10.1021/ja8048755.
14. Cruz M, Morales J, Espinos J, Sanz J. XRD, XPS and Sn NMR study of tin sulfides obtained by using chemical vapor transport methods. J Solid State Chem. 2003;175:359–65. https://doi.org/10.1016/s0022-4596(03)00329-3.
15. Lefebvre-Devos I, Olivier-Fourcade J, Jumas JC, Lavela P. Lithium insertion mechanism in SnS_2. Phys Rev B. 2000;61:3110–6. https://doi.org/10.1103/physrevb.61.3110.
16. Choi N, Chen Z, Freunberger SA, Ji X, Sun Y, Amine K, et al. Challenges facing lithium batteries and electrical double-layer capacitors. Angew Chem Int Ed Engl. 2012;51:9994–10024. https://doi.org/10.1002/anie.201201429.
17. Courtney IA, McKinnon WR, Dahn JR. On the aggregation of tin in SnO composite glasses caused by the reversible reaction with lithium. J Electrochem Soc. 1999;146:59–68. https://doi.org/10.1149/1.1391565.
18. Kim HS, Chung YH, Kang SH, Sung Y-E. Electrochemical behavior of carbon-coated SnS_2 for use as the anode in lithium-ion batteries. Electrochim Acta. 2009;54:3606–10. https://doi.org/10.1016/j.electacta.2009.01.030.

19. Li X, Chu L, Wang Y, Pan L. Anchoring function for polysulfide ions of ultrasmall SnS_2 in hollow carbon nanospheres for high performance lithium–sulfur batteries. Mater Sci Eng B. 2016;205:46–54. https://doi.org/10.1016/j.mseb.2015.12.002.
20. Zhang H, Yang D, Li S, Ji Y, Ma X, Que D. Hydrothermal synthesis of flower-like $Bi_2S_3$with nanorods in the diameter region of 30 nm. Nanotechnology 2004;15:1122–5. https://doi.org/10.1088/0957-4484/15/9/003.
21. Wang C, Tang K, Yang Q, Qian Y. Raman scattering, far infrared spectrum and photoluminescence of SnS_2 nanocrystallites. Chem Phys Lett. 2002;357:371–5. https://doi.org/10.1016/s0009-2614(02)00495-5.
22. Hai B, Tang K, Wang C, An C, Yang Q, Shen G, et al. Synthesis of SnS_2 nanocrystals via a solvothermal process. J Cryst Growth. 2001;225:92–5. https://doi.org/10.1016/s0022-0248(01)01030-2.
23. Lin Z, Liu Z, Fu W, Dudney NJ, Liang C. Lithium polysulfidophosphates: a family of lithium-conducting sulfur-rich compounds for lithium–sulfur batteries. Angew Chem. 2013;125:7608–11. https://doi.org/10.1002/ange.201300680.
24. Zhou G, Tian H, Jin Y, Tao X, Liu B, Zhang R, et al. Catalytic oxidation of Li_2S on the surface of metal sulfides for Li–S batteries. Proc Natl Acad Sci U S A. 2017;114(5):840–5. https://doi.org/10.1073/pnas.1615837114.